https://doi.org/10.5194/gmd-2021-141
Preprint. Discussion started: 11 May 2021

Geoscientific Model Development Discussions

Influence on the Temperature Estimation by the Planetary Boundary Layer Scheme with Different Minimum Eddy Diffusivity in WRF v3.9.1.1

Hongyi Ding[1], Le Cao[1,*], Haimei Jiang[1], Wenxing Jia[1,2], Yong Chen[3], and Junling An[3]

[1]Key Laboratory for Aerosol-Cloud-Precipitation of China Meteorological Administration, Nanjing University of Information Science and Technology, Nanjing 210044, China
[2]Key Laboratory of Atmospheric Chemistry of CMA, Chinese Academy of Meteorological Sciences, Beijing 100081, China
[3]State Key Laboratory of Atmospheric Boundary Layer Physics and Atmospheric Chemistry, Institute of Atmospheric Physics, Chinese Academy of Sciences, Beijing 100029, China

Correspondence: L. Cao
(le.cao@nuist.edu.cn)

Abstract. The minimum eddy diffusivity (Kzmin) in the planetary boundary layer (PBL) scheme is able to influence the performance of the model in simulating meteorological parameters such as the temperature. However, detailed studies on the sensitivities of the simulated temperature to the settings of Kzmin are still lacking. Thus, in this study, we evaluated the performance of the ACM2 (Asymmetrical Convective Model, version 2) scheme in the WRF (Weather Research and Forecasting) model with different settings of Kzmin, in simulating the spatiotemporal distribution of the temperature in the region of Beijing, China. Five constant values as well as a function were implemented in the model to calculate Kzmin, and the simulation results with different settings of Kzmin were compared and analyzed. The results show that the increase of Kzmin leads to an elevation of the 2-m temperature, especially in the nighttime. We figured out that the deviation of the 2-m temperature at night is mainly caused by the different estimation of the turbulent mixing under stable conditions in simulation scenarios with different Kzmin settings. Moreover, the spatial distribution of the temperature deviation indicates that under various underlying surface categories, the change of Kzmin exerts a different influence on the prediction of the 2-m temperature, and the influence was found stronger during the nighttime than during the daytime, in plain areas than in mountain areas, in urban areas than in non-urban areas. In the nighttime of the urban areas, the influence on the simulated 2-m temperature brought about by the change of Kzmin was found the strongest. In addition, we found that the implementation of a functional type Kzmin in the ACM2 scheme helps to improve the performance of the model in capturing the diurnal change and the vertical distribution of the temperature in this region, compared with that using a constant Kzmin.

1 Introduction

The planetary boundary layer (PBL) refers to a thin layer at the bottom of the atmosphere, which responds to the change of the surface within one hour or less (Stull, 1988). Generally, the height of the PBL is variable in time and space, ranging from hundreds of meters to a few kilometers. Moreover, within the PBL, an obvious diurnal change of the temperature usually

https://doi.org/10.5194/gmd-2021-141
Preprint. Discussion started: 11 May 2021


Geoscientific Model Development Discussions

occurs, which is mainly caused by the warming and cooling of the ambient air by the ground surface during the daytime and the nighttime, through the turbulent mixing. Turbulence in the PBL is an important form of air motion, and plays a critical role in vertically diffusing momentum, heat, moisture, and pollutants (Du et al., 2020). Therefore, it is important to accurately estimate the effects brought about by the turbulence on the vertical mixing within the PBL in weather and air quality models.

In numerical models, the vertical mixing caused by the turbulence is usually parameterized using PBL closure schemes. An appropriate PBL scheme can precisely capture the properties of the turbulent mixing as well as the structure of the PBL. At present, many PBL schemes are implemented in numerical models, such as YSU (Hong et al., 2006), MYJ (Janjić, 1994), MRF (Hong and Pan, 1996), ACM (Pleim and Chang, 1992), QNSE (Sukoriansky and Galperin, 2008; Sukoriansky et al., 2006), and BouLac (Bougeault and Lacarrere, 1989). Generally, the PBL schemes can be classified into two types, local and non-local closure schemes. Local closure scheme, such as MYJ and BouLac, is also called K-theory (Stull, 1988). It usually determines the eddy diffusion coefficient from local prognostic variables such as the turbulent kinetic energy (TKE), local gradients of the wind speed and the potential temperature. However, in this type of the PBL scheme, the mixing caused by large eddies is usually not adequately taken into account. As a result, the local closure schemes frequently fail in simulating the unstable boundary layer (Stull, 1988). In order to overcome the shortcomings of the local closure schemes, many non-local closure schemes such as MRF, YSU and ACM have been proposed. In the MRF non-local closure scheme, a counter-gradient correction term is included (Hong and Pan, 1996), which represents a contribution from the large-scale eddies to the total fluxes of heat, momentum and moisture. Based on the comparison of the model results with the observational data, Hong and Pan (1996) suggested that the MRF scheme simulates a more realistic structure of the daytime boundary layer than the local closure scheme. After that, based on MRF, a modified scheme, named YSU scheme was proposed (Hong et al., 2006), which treats the entrainment process occurring at the top of the PBL explicitly. It was found that the use of the YSU scheme tends to increase the boundary layer mixing in the thermally induced free convection regime, but tends to decrease the mixing in the mechanically induced forced convection regime (Hong et al., 2006). Aside from these two non-local closure schemes, ACM (Asymmetrical Convective Model) scheme, which is proposed by Pleim and Chang (1992), is also a non-local PBL scheme that assumes that strongly buoyant plumes rise from the surface layer to all levels in the convective boundary layer. It is also assumed in ACM that the downward motion between each adjacent layer is a gradual subsidence process. It was reported that the ACM scheme is able to improve the accuracy of the model in capturing the diffusion of chemicals released from elevated sources (Pleim and Chang, 1992). Based on that, by combining the original ACM with a local eddy diffusion module, Pleim (2007a,b) proposed the ACM2 scheme, to better represent both the super-grid and sub-grid components of the turbulent mixing in the convective boundary layer. It was found that the addition of the local eddy diffusion module into the original ACM exerts a significant impact on quantities that have large surface fluxes, such as the momentum and the heat (Pleim, 2007a,b).

Many researchers have evaluated the performance of available PBL closure schemes under different meteorological conditions (Hu et al., 2010; Xie et al., 2012; Madala et al., 2014; Banks et al., 2016; Gunwani and Mohan, 2017). Generally, they found that during the PBL collapse and the nighttime, the PBL schemes are difficult to precisely capture the change of meteorological parameters such as the temperature. Moreover, they attributed the reasons for the biases to three aspects: (1) Inaccurate calculation of the surface cooling rate. Chaouch et al. (2017) intercompared the performance of seven different PBL schemes

https://doi.org/10.5194/gmd-2021-141
Preprint. Discussion started: 11 May 2021


Geoscientific Model Development Discussions

in WRF (Weather Research and Forecasting) model (Skamarock et al., 2008) under foggy conditions in United Arab Emirates, and they found a cold bias in the 2-m air temperature during the PBL collapse and the nighttime, which reflects an overestimation of the surface cooling rate. Cuchiara et al. (2014) employed the WRF-Chem (WRF with Chemistry) model (Grell et al., 2005) to analyze the differences in the ozone prediction by four PBL schemes (YSU, ACM2, MYJ, QNSE). In their study, by comparing the model results with the observations, they found that the YSU scheme is in the best agreement with the observed values of ozone. Morevover, it was found by Cuchiara et al. (2014) that all these four PBL schemes predict a lower surface cooling rate, thus leading to an underestimation of the temperature by 2-3 K during the PBL collapse and the nighttime. (2) Unrealistic thermal coupling between the ambient air and the underlying surface in simulations. Udina et al. (2016) studied the vertical structure of a neutral and a stable PBL using the WRF-LES (WRF with Large Eddy Simulation) modeling system (Moeng et al., 2007). They suggested that in the model, the calculated thermal coupling at the surface is unrealistically large. As a result, the rate difference between the molecular thermal conduction and the vertical eddy diffusion is underestimated, leading to a lower prediction of the air temperature near the cooling surface in simulations. It also leads to a formation of a more stable boundary layer, compared to the observations. (3) Difference in internal properties of the PBL schemes. Shin and Hong (2011) numerically investigated the PBL properties using five PBL schemes (YSU, ACM2, MYJ, QNSE, BouLac) in WRF for a day in the Cooperative Atmosphere-Surface Exchange Study (CASES-99) field campaign (Poulos et al., 2002). They found that the simulated surface temperature and the 2-m temperature in the nighttime given by these five PBL schemes show positive biases, compared with the observations, and they stated that the values of the minimum eddy diffusivity given in these PBL schemes are different, which might influence the simulation results.

The minimum eddy diffusivity (Kz_0 or called Kzmin) is a small value to fix the estimation of the vertical eddy diffusivity (Kz) by the PBL closure schemes. It denotes a very weak vertical diffusion in the free atmosphere or in a strongly stable boundary layer that cannot be resolved by the model. Li and Rappenglueck (2018) investigated the causes behind the nighttime ozone biases in a simulation of the ground-level ozone in southeast Texas, US using the ACM2 scheme in CMAQ (Byun and Schere, 2006). They also compared the results using two different Kzmin settings. One is that the Kzmin is set as a constant value 1 $m^2\ s^{-1}$ across the modeling domain, and the other setup is that Kzmin is computed by a formula so that it resides in a value range of 0.01-1.0 $m^2\ s^{-1}$. They found that using the formula computed Kzmin lowers the nighttime vertical mixing, and the average ozone bias is reduced compared with the alternative Kzmin setting. Their conclusions suggested that the setup of Kzmin is capable of changing the simulation results of the model. Nielsen-Gammon et al. (2010) evaluated the role of many parameters in the ACM2 scheme using WRF model, and they found that the variation of Kzmin exerts a significant impact on the simulated temperature in the lower troposphere, especially at night. Moreover, in the upper troposphere, different values of Kzmin would cause a change in the intensity of the vertical mixing. As a result, different vertical profiles of the temperature and the water vapor are given in simulations using various Kzmin values, leading to a different prediction of cloud patterns and shortwave radiation.

However, to the present, detailed studies on the sensitivities of the temperature prediction to the settings of Kzmin are still lacking. The reasons causing the deviations of the temperature in simulations brought by the change of Kzmin also need clarified. In addition, the effects of changing Kzmin on the temperature under different categories of the underlying surface

https://doi.org/10.5194/gmd-2021-141
Preprint. Discussion started: 11 May 2021


Geoscientific Model Development Discussions

are also unclear. Thus, in this study, we performed a WRF model simulation on the meteorological field of the region near Beijing, China, and examined the impact exerted by the change of Kzmin on the simulated temperature. We also tried to figure out the mechanism for the change of the simulated temperature. By performing this numerical study, the role of Kzmin in the prediction of temperature in Beijing area of China can be clarified, which helps to determine the appropriate setup of Kzmin in temperature simulations across this region, and is also capable of improving the behavior of the PBL scheme in capturing the boundary layer properties in this area.

The structure of the paper is as follows. In Section 2, we described the observational data, model settings and the PBL scheme used in the present study. In Section 3, simulation results and the related discussions are given. At last, major conclusions achieved in the present study are presented in Section 4. Future work is also prospected in this section.

2 Observational Data and Model Settings

In the present study, we first evaluated the performance of the PBL scheme (ACM2) with different Kzmin values in simulating temperature, by comparing with the observational data, and then assessed the connection between the differences in the temperature simulations and the value of Kzmin. At last, we used a function to calculate Kzmin and examined the performance of ACM2 with this function by comparing with that using a constant Kzmin ($0.01\ \mathrm{m^2\ s^{-1}}$).

2.1 Observational Data

The observational data used in this study are provided by the Institute of Atmospheric Physics, Chinese Academy Sciences (IAP, CAS), obtained by a meteorological observation tower and an observational system of surface meteorological parameters. The information of the tower and the system is as follows.

The meteorological observation tower of IAP was built in 1979, and consistently serves studies on air pollution, atmospheric boundary layer, and atmospheric turbulent diffusion. The tower is located at 39°58′N, 116°22′E and has a height of 325 m. A 15-level (8, 15, 32, 47, 63, 80, 102, 120, 140, 160, 180, 200, 240, 280, 320 meters) meteorological gradient observation system is instrumented on the tower, and provides data including wind speed, wind direction, temperature and moisture. The time resolution of the data is 10 minutes.

The observational system of surface meteorological parameters is instrumented next to the tower and provides the surface data including temperature, relative humidity, pressure, radiation, precipitation, wind speed and direction. The time resolution of these data is 30 minutes.

2.2 Model Description

In this study, we adopted the model WRF-ARW (Advanced Research WRF) version 3.9.1.1 to simulate the meteorological field of the region near Beijing, China. WRF is a mesoscale numerical weather forecasting system designed for atmospheric research and operational forecasting applications. The ARW version is developed and maintained by NCAR (National Center for Atmospheric Research) and is often used for scientific research. In the present study, the WRF model was adapted to

https://doi.org/10.5194/gmd-2021-141
Preprint. Discussion started: 11 May 2021

Geoscientific Model Development Discussions
Open Access
EGU

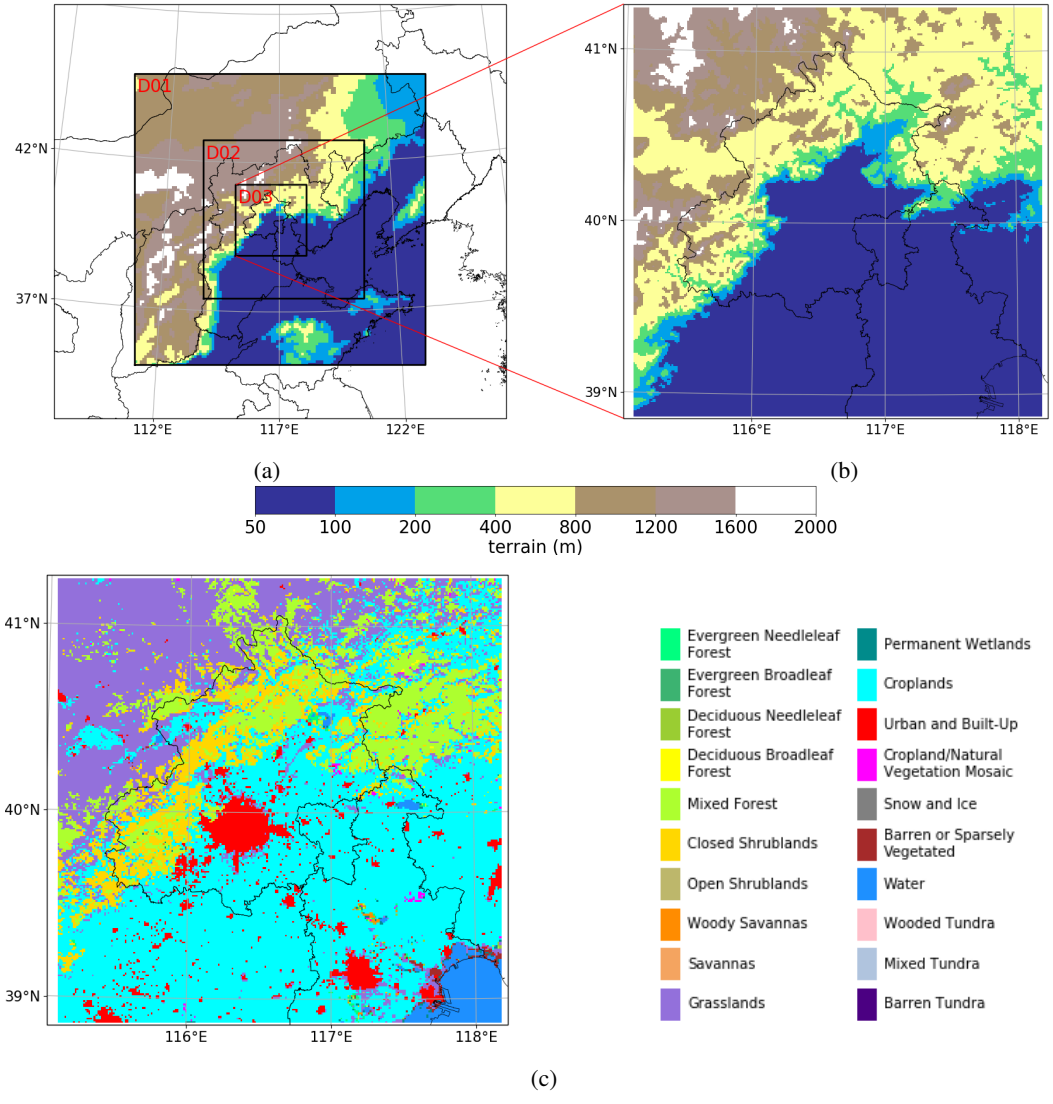

Figure 1. Description of (a) the locations of three model domains, (b) an enlarged drawing of the terrain belonging to the innermost domain (i.e. D03), and (c) the spatial distribution of the land-use categories within D03.

the conditions of Beijing and its surrounding areas (Fig. 1). Three model domains (D01, D02, and D03) were defined (see Fig. 1a), with horizontal grid spacing of 9 km (119×119 grid nodes), 3 km (196×193 grid nodes) and 1 km (259×259 grid nodes), respectively. Along the vertical direction, 48 levels were distributed. The terrain and the categories of the land use in the innermost domain (i.e. D03) are shown in Fig. 1(b) and (c). It is seen that there are mountains in the north (Yanshan Mountains) and the west (Taihang Mountains) of this area, and the North China Plain is located in the southeast of this studied domain. The boundary between the mountain area and the plain area is sharp. In the present study, two time periods (Jan. 8-15 and Jan.

https://doi.org/10.5194/gmd-2021-141
Preprint. Discussion started: 11 May 2021

Geoscientific Model Development Discussions

Table 1. Parameterizations used in the present model.

Namelist option	Description	Reference
mp_physics	Purdue Lin scheme	Chen and Sun (2002)
ra_lw_physics	RRTM scheme	Mlawer et al. (1997)
ra_sw_physics	Dudhia scheme	Dudhia (1989)
sf_sfclay_physics	MM5 scheme	Zhang and Anthes (1982)
sf_surface_physics	Noah land surface model	Chen and Dudhia (2001)
bl_pbl_physics	ACM2 scheme	Pleim (2007a,b)
cu_physics	Grell 3D scheme (Domain 1 and 2)	Grell and Dévényi (2002)

20-24, 2014) were simulated. In these two time periods, the concentration of $PM_{2.5}$ (particulate matters with diameters smaller than 2.5 μm) accumulates (see Fig. S1 of the supplementary material), which reflects relatively stagnant weather conditions of this area. The initial and the boundary conditions were given by the $1^\circ \times 1^\circ$ National Centers for Environmental Prediction (NCEP) Global Forecast System (GFS) Final (FNL) analysis data (National Centers for Environmental Prediction, National Weather Service, NOAA, U.S. Department of Commerce, 2000) and the Moderate Resolution Imaging Spectroradiometer (MODIS) dataset (Broxton et al., 2014) including 20 categories of the land use. The parameterizations used in the present model are listed in Table 1.

2.2.1 ACM2 PBL Scheme

In this study, we adopted the ACM2 scheme as the PBL scheme. The reason for choosing ACM2 is that this scheme is included in many numerical models such as WRF (Skamarock et al., 2008) and CMAQ (Byun and Schere, 2006), and the settings of Kzmin in this scheme are given differently in these models, which will be described in a later context. The form of the scalar transport equation in ACM2 is as follows (Pleim, 2007a,b):

$$\frac{\partial C_i}{\partial t} = f_{conv} M u C_1 - f_{conv} M d_i C_i + f_{conv} M d_{i+1} C_{i+1} \frac{\Delta z_{i+1}}{\Delta z_i} + \frac{\partial}{\partial z}\left[K_c (1 - f_{conv}) \frac{\partial C_i}{\partial z}\right] \quad (1)$$

https://doi.org/10.5194/gmd-2021-141
Preprint. Discussion started: 11 May 2021

Geoscientific Model Development Discussions
Open Access
EGU

Table 2. Scenarios simulated in the present study, with different setup of Kzmin in the ACM2 scheme.

Type	Kzmin ($\mathrm{m^2\ s^{-1}}$)	Name
Constant	0.01	ACM2_0.01
	0.2	ACM2_0.2
	0.5	ACM2_0.5
	0.8	ACM2_0.8
	1.0	ACM2_1.0
Function	0.01~1.0	ACM2_CMAQ

$$f_{conv} = \frac{K_h \gamma_h}{K_c \gamma_h - K_h \frac{\partial \theta}{\partial z}} \tag{2}$$

where C_i is the predicted variable such as the potential temperature in the i-th layer. Mu is the mixing rate of the non-local upward convection, and Md is the rate of the non-local downward mixing from the i-th layer to the $(i-1)$-th layer. Δz_i is the thickness of the i-th model layer. f_{conv} is a ratio factor weighting different contributions from non-local mixing and local mixing, and θ in Eq. (2) is the potential temperature. When the boundary layer is stable or neutral, the ACM2 scheme is mostly dominated by the local transport process, which is represented by the last term in the right hand side of Eq. (1). By adding the local transport term, the ACM2 scheme improves upon the ACM scheme in capturing the upward turbulent transport process within the boundary layer (Pleim, 2007a,b).

2.2.2 Setup of Kzmin in ACM2

In the ACM2 scheme instrumented in the WRF model, Kzmin is set as 0.01 $\mathrm{m^2\ s^{-1}}$ by default. In contrast to that, in other numerical models such as CMAQ (Byun and Schere, 2006), Kzmin is usually given a value between 0.001 and 1.0 $\mathrm{m^2\ s^{-1}}$. Thus, in order to clarify the difference in simulation results caused by the variation of Kzmin, five simulation scenarios with different constant values of Kzmin were conducted in the present study (see Tab. 2). In addition, we also performed a simulation using a function to determine Kzmin (i.e. ACM2_CMAQ in Tab. 2). This function was taken from the CMAQ model, shown as follows:

$$Z \leq KZMAXL : \mathrm{Kzmin} = 0.01 + (1 - 0.01)PURB \tag{3}$$

$$Z \geq KZMAXL : \mathrm{Kzmin} = 0.01 \tag{4}$$

https://doi.org/10.5194/gmd-2021-141
Preprint. Discussion started: 11 May 2021


Geoscientific Model Development Discussions

where:

$$KZMAXL = 500.0\ (\mathrm{m}) \tag{5}$$

$$LU\_INDEX = LU\_INDEX(\mathrm{Water}) : PURB = 0 \tag{6}$$

$$LU\_INDEX \neq LU\_INDEX(\mathrm{Water}) : \quad PURB = \frac{Landusef(\mathrm{Urban})}{1 - Landusef(\mathrm{Water})} \tag{7}$$

In Eqs. (3)–(7), Z is the height of the layer, and $KZMAXL$ is a prescribed height above which the atmosphere would not be significantly affected by the change of the surface properties. $PURB$ is a percentage ratio of the urbanization. LU_INDEX is an index representing the category of the land use. $Landusef$ is a fraction of each land-use category in the grid cell. By using the function described in Eqs. (3)–(7), the range of Kzmin given in the model is between 0.01 and 1 $\mathrm{m^2\ s^{-1}}$. Moreover, for completely non-urban areas (i.e. $PURB = 0.0$), the value of Kzmin is 0.01 $\mathrm{m^2\ s^{-1}}$, which is the same to the default value used in the ACM2 scheme of the WRF model. We then compared the performance of ACM2 adopting this function with that using a constant Kzmin (0.01 $\mathrm{m^2\ s^{-1}}$) in simulating the temperature in the region of Beijing.

2.3 Evaluation Criterion

In order to evaluate the performance of the model with different settings of Kzmin, three statistical metrics, index of agreement (IOA) (Willmott, 1982), root mean square error (RMSE), and correlation coefficient (R) were implemented. These parameters are calculated as:

$$\mathrm{IOA} = 1 - \left[\frac{\sum_{i=1}^{N} (P_i - O_i)^2}{\sum_{i=1}^{N} \left(|P_i - \overline{O}| + |O_i - \overline{O}| \right)^2} \right] \tag{8}$$

$$\mathrm{RMSE} = \sqrt{\frac{\sum_{i=1}^{N} (P_i - O_i)^2}{N}} \tag{9}$$

$$\mathrm{R} = \frac{\sum_{i=1}^{N} \left(P_i - \overline{P}\right)\left(O_i - \overline{O}\right)}{\sqrt{\sum_{i=1}^{N} \left(P_i - \overline{P}\right)^2} \sqrt{\sum_{i=1}^{N} \left(O_i - \overline{O}\right)^2}} \tag{10}$$

https://doi.org/10.5194/gmd-2021-141
Preprint. Discussion started: 11 May 2021


Geoscientific Model Development Discussions

where N is the number of data; O is the observed value and P is the value predicted by the model. $\overline{O}$ and $\overline{P}$ denote the average values of these variables. RMSE and R are common statistical parameters and IOA is a metrics evaluating the fitness between model predictions and observations. When IOA is equal to 1, it represents a perfect match, while IOA=0 denotes that no agreement is achieved.

3 Results and Discussions

In Section 3.1, we show the impact of changing Kzmin on the 2-m temperature and discover the reasons for the change of the 2-m temperature. In Section 3.2, the impact of changing Kzmin under different underlying-surface categories is shown. In Section 3.3, we compare the performance of ACM2 adopting the function described in Eqs. (3)–(7) with the results using the constant Kzmin 0.01 $\mathrm{m^2\ s^{-1}}$.

3.1 Impact of Changing Kzmin on 2-m Temperature

Figure 2 shows the diurnal mean time series of the temperature at 2 m (T2), the surface skin temperature (TSK), and the temperature at the first model layer (T_level1) at the observation site, predicted by ACM2 with different Kzmin constant values. In Fig. 2(a), it is seen that the highest T2 appears at approximately 15 LST (local standard time). At this time, the average T2 estimated by ACM2_0.01 and ACM2_1.0 are 1.81 °C and 2.25 °C, and T2 estimated by the other scenarios are between these two values. In contrast to that, the lowest T2 appears at about 8 LST. At this time, the average T2 predicted by ACM2_0.01 and ACM2_1.0 are -6.69 °C and -4.13 °C. Among these scenarios, ACM2_0.01 consistently predicts the lowest T2. Moreover, it was found that the simulated T2 elevates with the increase of Kzmin. In addition, the difference of T2 between these five scenarios is smaller at a higher T2, while the difference becomes larger at a lower T2. As a result, the diurnal variation of T2 is reduced with the increase of Kzmin.

We then investigated the reasons causing the difference in the simulated T2 between these scenarios. In the model, T2 is interpolated by the surface skin temperature (TSK) and the temperature at the first model layer (T_level1) using the similarity theory (Monin and Obukhov, 1954; Stull, 1988). We thus show the diurnal mean time series of TSK and T_level1 estimated by different Kzmin values (see Fig. 2b and c). It can be seen that during the nighttime, both TSK and T_level1 increase remarkably with the increase of Kzmin, which is similar to the temporal behavior of T2. This finding is also in partly agreement with the conclusions of Steeneveld et al. (2006), who stated that TSK increases substantially with an enhanced vertical mixing during the nighttime. However, from the temporal change of these two temperatures, we cannot figure out whether the difference in T2 is mostly caused by the change of the surface temperature (i.e. TSK) or the temperature in the atmosphere (i.e. T_level1), because of the interaction between the surface and the atmosphere. Therefore, we continue to discover the dominant factor causing the change of TSK and T_level1, respectively.

We first try to infer the reason causing the difference in TSK, from the energy balance equation. In the Noah land surface model (Chen and Dudhia, 2001; Xie et al., 2012) used in this study, when neglecting the precipitation and the snow accumulated

https://doi.org/10.5194/gmd-2021-141
Preprint. Discussion started: 11 May 2021

Geoscientific Model Development Discussions
Open Access
EGU

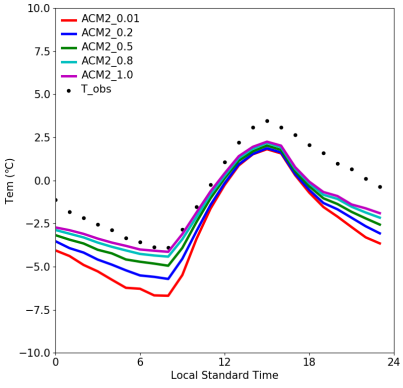

(a) temperature at 2 m (T2)

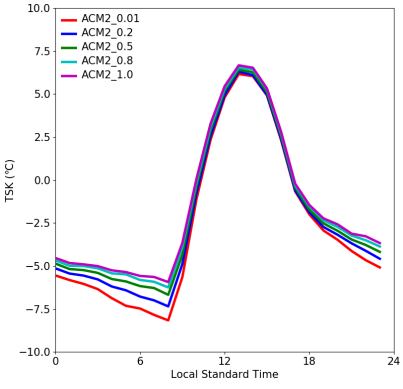

(b) surface skin temperature (TSK)

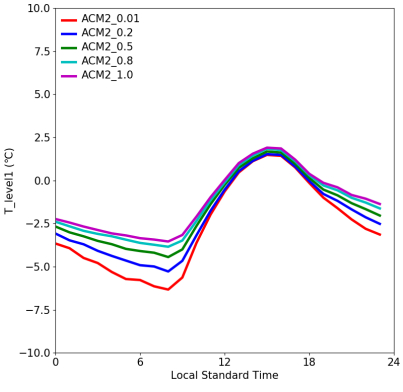

(c) temperature at the first model layer (T_level1)

Figure 2. Diurnal mean time series of (a) the temperature at 2 m (T2), (b) the surface skin temperature (TSK), and (c) the temperature at the first model layer (T_level1), predicted by the ACM2 scheme with different Kzmin constant values.

https://doi.org/10.5194/gmd-2021-141
Preprint. Discussion started: 11 May 2021


Geoscientific Model Development Discussions
Open Access
EGU

on the surface, the form of the energy balance equation is:

$$(1-\alpha)\,S\downarrow + L\downarrow - L\uparrow + G - HFX - LH = 0 \tag{11}$$

where α is the albedo of the underlying surface. $S\downarrow$ is the downward flux of the shortwave radiation. $L\downarrow$ is the downward flux of the longwave radiation emitted by the cloud and the atmosphere, and $L\uparrow$ is the upward flux of the longwave radiation emitted by the ground surface. G is the ground heat flux, and it is positive when heat transfers from the soil to the surface. HFX is the sensible heat flux, and LH is the latent heat flux at the surface. HFX and LH are positive when the heat transfers from the surface to the atmosphere. We then combined $L\downarrow$ and $L\uparrow$ as a net longwave flux ($NL = L\downarrow - L\uparrow$). As a result, Eq. (11) becomes:

$$(1-\alpha)\,S\downarrow + G + NL - HFX - LH = 0 \tag{12}$$

Thus, five factors ($S\downarrow$, G, NL, HFX and LH) need to be evaluated for the difference of TSK between these simulation scenarios. Among these factors, we can first eliminate the shortwave radiation $S\downarrow$ as the dominant factor for the deviation in TSK. It is because that in our simulation, the difference of TSK is more obvious during the nighttime (see Fig. 2b). However, the shortwave radiation is negligible at night. It thus denotes the unimportant role of the shortwave radiation $S\downarrow$ in the deviation of TSK. Then four factors (G, NL, LH and HFX) need to be evaluated. Figure 3 shows the temporal profiles of the deviations (ACM2_0.2 minus ACM2_0.01, ACM2_0.5 minus ACM2_0.01, ACM2_0.8 minus ACM2_0.01, ACM2_1.0 minus ACM2_0.01) in G, NL, LH and HFX given by the model simulations. From Fig. 3(a), we can see that during the nighttime, the negative deviation of the ground heat flux G becomes larger when Kzmin increases, denoting that G is reduced with the increase of Kzmin in the nighttime. Because lower G in the nighttime represents that less heat is transferred from the soil to the surface, which cannot lead to a higher TSK, the heat flux from the soil to the surface, G, can also be eliminated as the dominant factor causing the change of TSK during the nighttime. Then, from Fig. 3(b), it can be seen that during the nighttime, the negative deviation of the net longwave radiation (i.e. NL) becomes larger when Kzmin increases, which means that the value of NL also gets reduced when Kzmin increases. Because lower NL means that the surface loses more longwave radiation energy, which cannot lead to a higher TSK. It can thus be deduced that the change in the net longwave flux NL is also not the major factor causing the growth of the TSK difference. Figure 3(c) shows that during the nighttime, there is no obvious difference in the latent heat flux LH between these scenarios. Therefore, LH can also be screened out. At last, from Fig. 3(d), it was found that during the nighttime, the negative bias in the sensible heat flux HFX becomes larger when Kzmin increases, which means that HFX is reduced when Kzmin increases. Because lower HFX at night means that more heat is transferred from the atmosphere to the underlying surface, which is capable of increasing TSK, we can thus conclude that the difference in the sensible heat transported from the atmosphere to the ground among these simulation scenarios causes the different growth of TSK during the nighttime in the present simulations.

We then tried to reveal the reasons for the change of the air temperature at the first model layer (i.e. T_level1), caused by the modifications of Kzmin in the model. Figure 4 shows hourly averaged vertical profiles of the potential temperature predicted by ACM2 using different Kzmin at 8 LST and 15 LST. From Fig. 4(a), we found that at 8 LST, the potential temperature

https://doi.org/10.5194/gmd-2021-141
Preprint. Discussion started: 11 May 2021

Geoscientific Model Development Discussions
Open Access
EGU

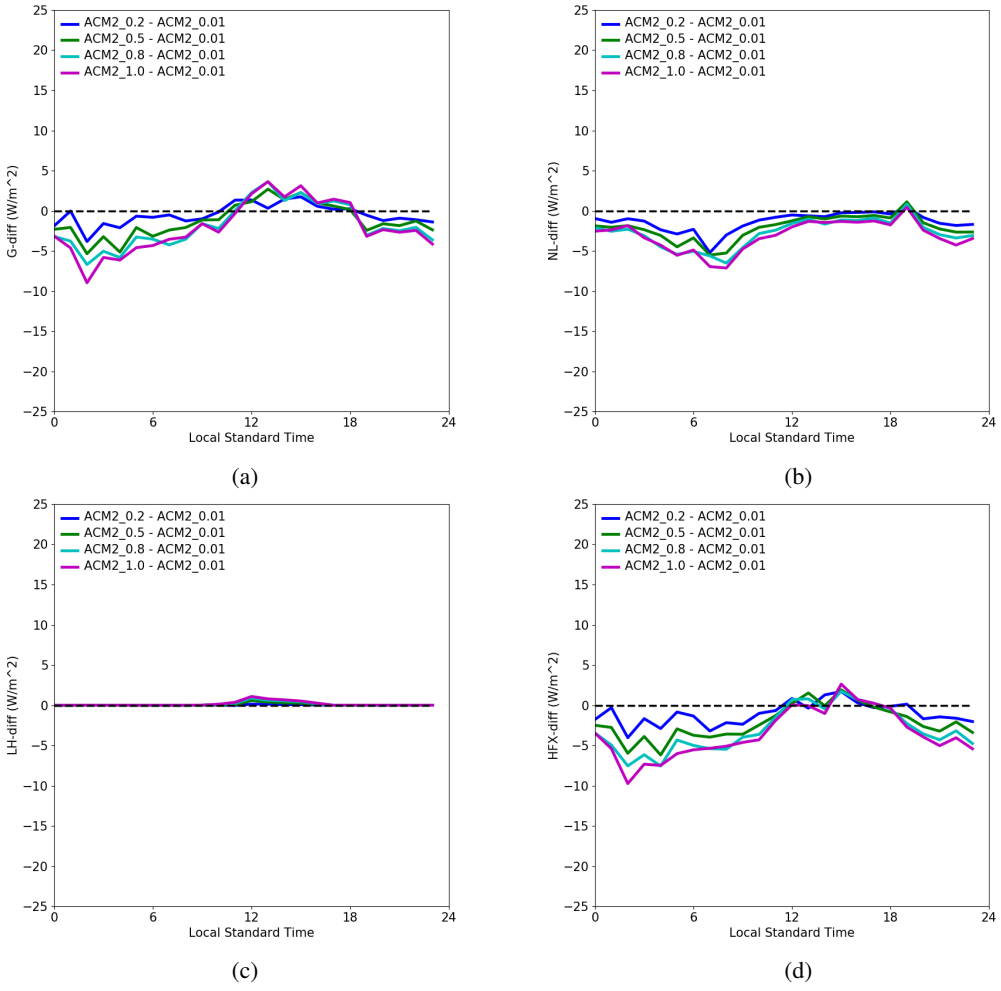

Figure 3. Diurnal mean time series of deviations (based on ACM2_0.01) in (a) the ground heat flux G, (b) the net longwave flux NL, (c) the latent heat flux LH and (d) the sensible heat flux HFX at the surface.

difference at the first model layer is the largest between these five scenarios. When Kzmin increases, the predicted near-surface potential temperature elevates. It is consistent with the conclusion of Nielsen-Gammon et al. (2010) saying that Kzmin exerts the largest effect during the nighttime, and the variation of Kzmin is positively correlated with the change of the near-surface potential temperature. Moreover, seen from Fig. 4(a), the potential temperature difference becomes smaller at a higher altitude. Above the height of 400 m, the potential temperature profiles predicted by these five scenarios are almost identical. Therefore, when Kzmin increases, the vertical gradient of the mean potential temperature decreases at this time. It is because that during the nighttime, the PBL becomes stable, under which condition the turbulence is too weak to be resolved by the model. The settings of Kzmin thus exerts a relatively greater influence on Kz. As a result, the increase of Kzmin would lead to a significant

https://doi.org/10.5194/gmd-2021-141
Preprint. Discussion started: 11 May 2021

Geoscientific Model Development Discussions

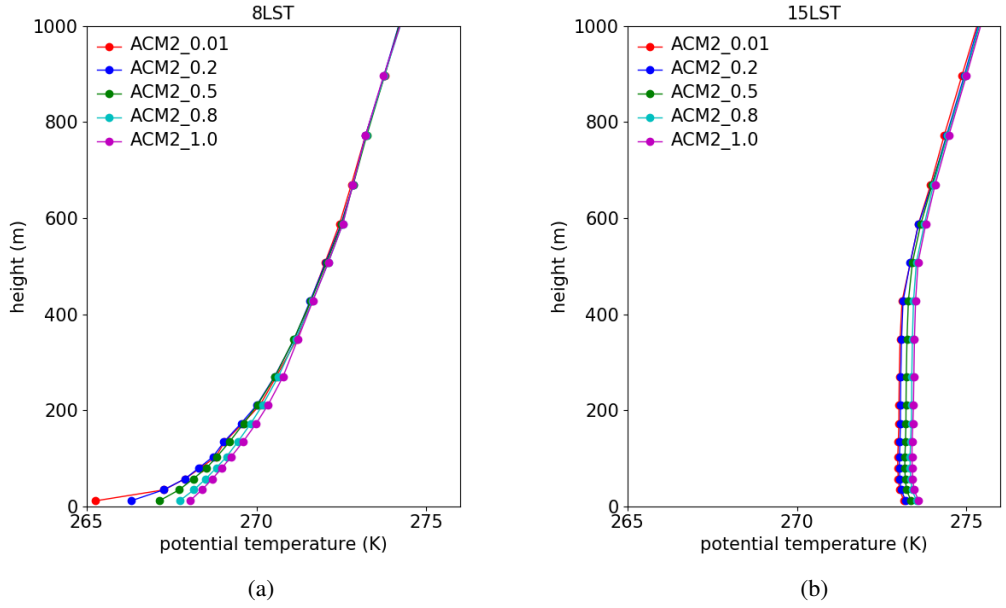

Figure 4. Hourly averaged vertical profiles of the potential temperature predicted by the ACM2 scheme with different Kzmin values at (a) 8 LST and (b) 15 LST.

enhancement of the vertical mixing during the nighttime. This enhanced vertical mixing then causes a more uniform vertical distribution of the potential temperature within the PBL and thus a prediction of a smaller temperature gradient below the top of the PBL. This conclusion is also in accordance with that of Nielsen-Gammon et al. (2010), who stated that the minimum vertical diffusivity is negatively correlated with the temperature gradient during the nighttime. With respect to the predicted vertical profile of the potential temperature at 15 LST, it was found in Fig. 4(b) that larger Kzmin also estimates a higher potential temperature. It is because that an enhanced vertical mixing in the daytime would cause a stronger entrainment of the air with higher potential temperature from the upper layer into the boundary layer, resulting in a warmer boundary layer (Hu et al., 2010). Moreover, it was found in Fig. 4(b) that the temperature profiles predicted by these five scenarios at this time are closer to each other than those at 8 LST. The reason is that during the daytime, the turbulent intensity is strong so that the change of Kzmin has a relatively minor impact on the eddy diffusivity Kz as well as the vertical distribution of the temperature.

Thus, based on the investigations of TSK and T_level1 discussed above, we can conclude the mechanism causing the remarkable change of T2 between the simulation scenarios with different Kzmin settings during the nighttime, shown in Fig. 2(a). When Kzmin increases, the vertical mixing in the nighttime is significantly enhanced. As a result, the near-surface temperature in the boundary layer (i.e. T_level1) is elevated due to the enhanced mixing of the warm air from the atmosphere above. The higher near-surface temperature thus leads to a reduction of the sensible heat flux at the surface (i.e. HFX) in the nighttime and results in an increase of the surface skin temperature (TSK). Because the 2-m air temperature (i.e. T2) in the model is interpolated by TSK and T_level1, the elevation of Kzmin thus causes the increase of T2.

https://doi.org/10.5194/gmd-2021-141
Preprint. Discussion started: 11 May 2021

Geoscientific Model Development Discussions
Open Access
EGU

3.2 Impact of Changing Kzmin under Different Underlying Surface Categories

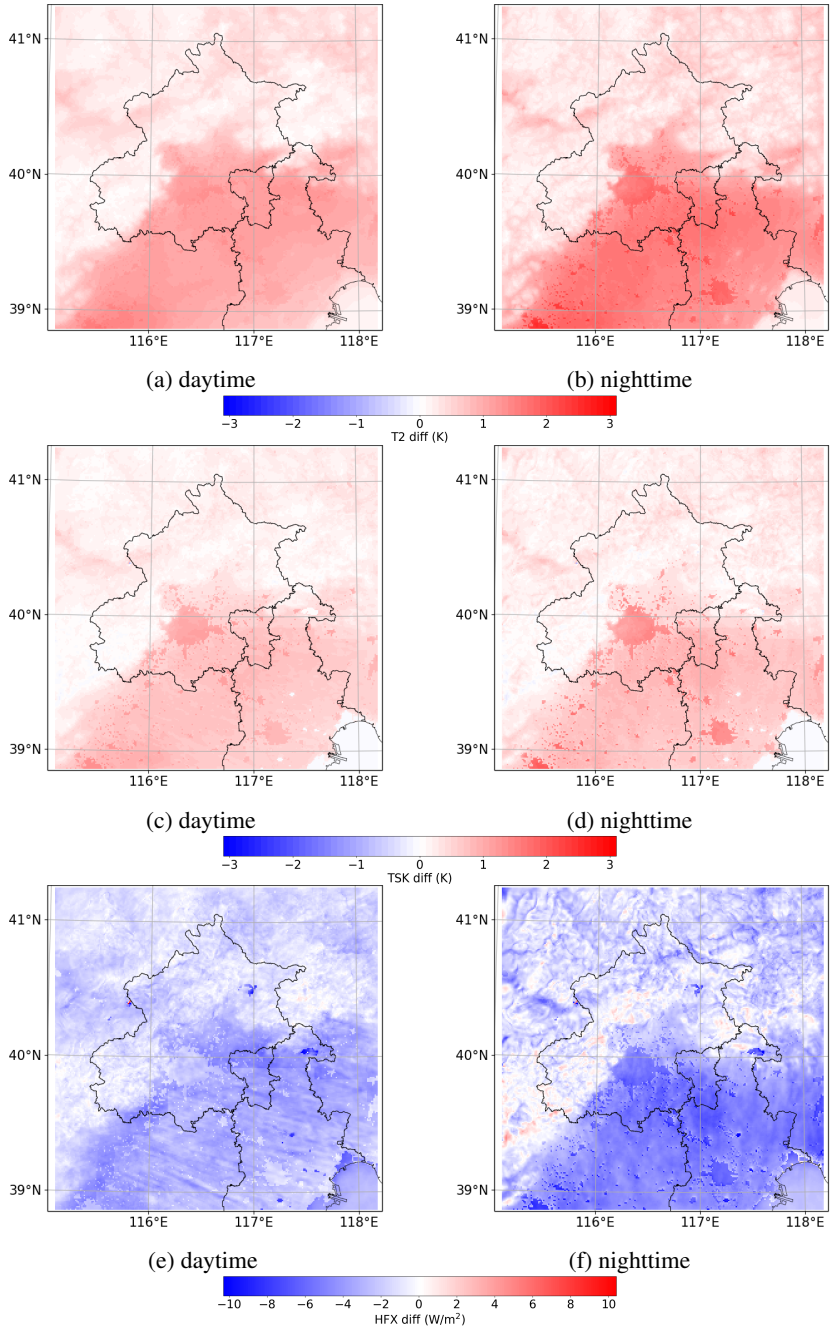

Figure 5. Spatial distribution of the mean difference (ACM2_1.0 minus ACM2_0.01) in (a, b) the 2-m temperature (T2), (c, d) the surface skin temperature (TSK), and (e, f) the sensible heat flux (HFX) over the daytime (left row) and the nighttime (right row).

https://doi.org/10.5194/gmd-2021-141
Preprint. Discussion started: 11 May 2021


Geoscientific Model Development Discussions

The spatial distribution of the time averaged difference (ACM2_1.0 minus ACM2_0.01) in T2, TSK and HFX over the daytime and the nighttime is shown in Fig. 5. From Fig. 5(a) and (b), we can figure out three distinct features about the influence of increasing Kzmin on T2. First, the difference of T2 is mostly larger in plain areas than in mountain areas, which means that the increase of Kzmin has a stronger influence on T2 in plain areas than in mountain areas. The reason for the relatively weaker impact of changing Kzmin in mountain areas than in plain areas might be that the complex terrain of the mountain areas tends to generate larger eddies and thus induces a stronger turbulent mixing, which is represented by the larger turbulent diffusivity belonging to the mountain areas (shown in Fig. S2 of the supplement). As a result, elevating Kzmin in the mountain areas exerts a relatively minor influence on the vertical mixing in the boundary layer as well as the simulated T2. Second, it was found that in plain areas, the difference of T2 is mostly larger during the nighttime than during the daytime, denoting a stronger impact on T2 exerted by the increase of Kzmin during the nighttime than during the daytime. Third, from the comparison between Fig. 5(a) and (b), it was found that during the nighttime, the difference of T2 is substantially larger in urban and built-up areas than that in areas with other land-use categories. But during the daytime, the difference is smaller. It means that the increase of Kzmin has the strongest influence on T2 in urban and built-up areas during the nighttime.

Regarding to TSK, in Fig. 5(c) and (d), we can see that these three features are also valid. The difference of TSK is larger in plain areas than in mountain areas, during the nighttime than during the daytime, in urban areas than in areas with other land-use categories at night. But the difference of TSK is less than that of T2, indicating that the increase of Kzmin exerts a less influence on TSK than on T2.

From Fig. 5(e) and (f) we can see that in most areas, when Kzmin increases, HFX decreases during both the daytime and the nighttime, which represents that less heat is transferred from the surface to the atmosphere or larger amount of heat is transported from the atmosphere to the surface, respectively. Moreover, it was shown that the difference of HFX is larger in plain areas than in mountain areas. In addition, by comparing Fig. 5(e) and (f), we found the boundary of the urban areas clearly discernible during the nighttime but unclear during the daytime. It denotes that in the nighttime, the effects of changing Kzmin on HFX in urban and non-urban areas are substantially different, while in the daytime, the effects are similar.

3.3 Performance of ACM2_CMAQ and ACM2_0.01

We then adopted a function described in Eqs. (3)–(7) to calculate Kzmin and compared the performance of the model (i.e. ACM2_CMAQ) with that using a constant Kzmin (ACM2_0.01). The diurnal mean time series of T2, TSK, HFX predicted by ACM2_CMAQ and ACM2_0.01 are shown in Fig. 6. From Fig. 6(a), we can see that T2 predicted by ACM2_CMAQ is consistently higher than that predicted by ACM2_0.01, although it still underestimates the observations. It is also shown that the difference in T2 between ACM2_CMAQ and ACM2_0.01 increases at a lower T2, and the difference attains the greatest when T2 reaches the lowest value in the morning. The difference in the minimum T2 between ACM2_CMAQ and ACM2_0.01 is 2.01 °C, while the deviation in the maximum T2 between these two scenarios is only 0.17 °C. As a result, the diurnal change of T2 using ACM2_CMAQ is smaller than that using ACM2_0.01. From Fig. 6(b), it is shown that the behavior of the predicted TSK belonging to these two scenarios is similar to that of T2. ACM2_CMAQ predicts a higher TSK than ACM2_0.01 especially at night and thus a smaller diurnal change of TSK. From Fig. 6(c), we found that the difference of HFX between

https://doi.org/10.5194/gmd-2021-141
Preprint. Discussion started: 11 May 2021

Geoscientific Model Development Discussions
Open Access
EGU

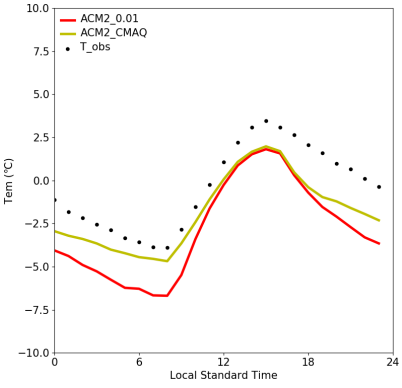

(a) temperature at 2 m (T2)

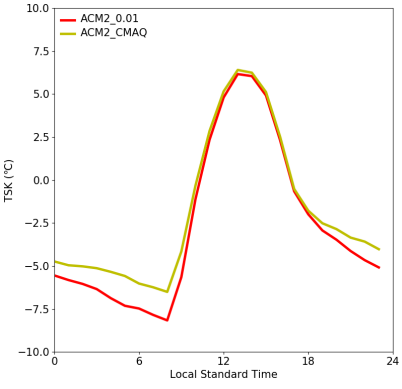

(b) surface skin temperature (TSK)

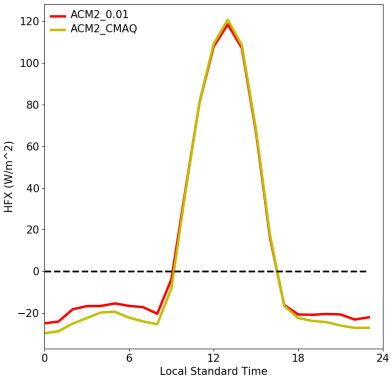

(c) sensible heat flux at the ground (HFX)

Figure 6. Diurnal mean time series of (a) T2, (b) TSK, and (c) HFX, predicted by ACM2_CMAQ and ACM2_0.01.

https://doi.org/10.5194/gmd-2021-141
Preprint. Discussion started: 11 May 2021

Geoscientific Model Development Discussions
Open Access
EGU

Table 3. Statistical performances of ACM2_0.01 and ACM2_CMAQ in simulating T2.

Scenarios	R	IOA	RMSE
ACM2_0.01	0.976	0.804	2.578
ACM2_CMAQ	0.975	0.894	1.552

ACM2_CMAQ and ACM2_0.01 is larger at a negative HFX, while the difference is negligible at a positive HFX. When HFX is negative, the value of HFX predicted by ACM2_CMAQ is lower than that predicted by ACM2_0.01. It means that in the night simulations using ACM2_CMAQ, more heat is transferred from the atmosphere to the ground, relative to the ACM2_0.01 scenario. It is caused by the enhanced vertical mixing within the boundary layer during the nighttime in the ACM2_CMAQ scenario, as the Kzmin value given in ACM2_CMAQ is higher than that in ACM2_0.01. Table 3 summarizes the statistical performances of these two scenarios in simulating T2. It was found that the correlation coefficients (R) of ACM2_CMAQ and ACM2_0.01 are close. However, the index of agreement (i.e. IOA) of ACM2_CMAQ is closer to 1.0 than that of ACM2_0.01, and RMSE of ACM2_CMAQ is smaller than that of ACM2_0.01, denoting that the simulated T2 of ACM2_CMAQ deviates less from the observation than that of ACM2_0.01. Thus, in the present study, ACM2_CMAQ performs better than ACM2_0.01 in simulating T2.

Figure 7 shows the hourly averaged vertical profiles of the potential temperature at 8 LST and 15 LST predicted by ACM2_0.01 and ACM2_CMAQ as well as the observations. It can be seen that at 8 LST, the difference of the potential temperature between these two simulation scenarios is remarkable near the ground. Below the height of 100 m, the potential temperature estimated by ACM2_CMAQ is higher than that estimated by ACM2_0.01, and the largest difference (more than 2 K) occurs in the lowest layer of the model. In contrast, between the heights of 100 m and 500 m, the potential temperature predicted by ACM2_CMAQ is slightly lower than ACM2_0.01. The potential temperature gradient estimated by ACM2_CMAQ is thus smaller than that estimated by ACM2_0.01 below the height of 500 m. This different prediction of the vertical gradient of the potential temperature is because that at 8 LST, the turbulent mixing is very weak so that Kzmin dominates Kz. Moreover, the value of Kzmin calculated by the function in ACM2_CMAQ is larger than that of ACM2_0.01 below the height of 500 m. Therefore, ACM2_CMAQ estimates a stronger vertical mixing, thus reducing the potential temperature gradient below the height of 500 m. In constrast to that, the profiles of the potential temperature predicted by these two scenarios are similar above the height of 500 m, which is because that the values of Kzmin above 500 m are equal in these two scenarios. By comparing the simulation results with the observations (see Fig. 7a), we found that ACM2_CMAQ estimates a closer potential temperature profile to the observations compared with ACM2_0.01, but it still overestimates the temperature gradient in the boundary layer at this time.

At 15 LST (see Fig. 7b), both the potential temperatures predicted by these two scenarios are about 2 K lower than the obervations. The potential temperature predicted by ACM2_CMAQ is slightly higher than that predicted by ACM2_0.01 below the height of 500 m. Above 500 m, there is only a minor difference between ACM2_0.01 and ACM2_CMAQ. The reason is

https://doi.org/10.5194/gmd-2021-141
Preprint. Discussion started: 11 May 2021

Geoscientific Model Development Discussions

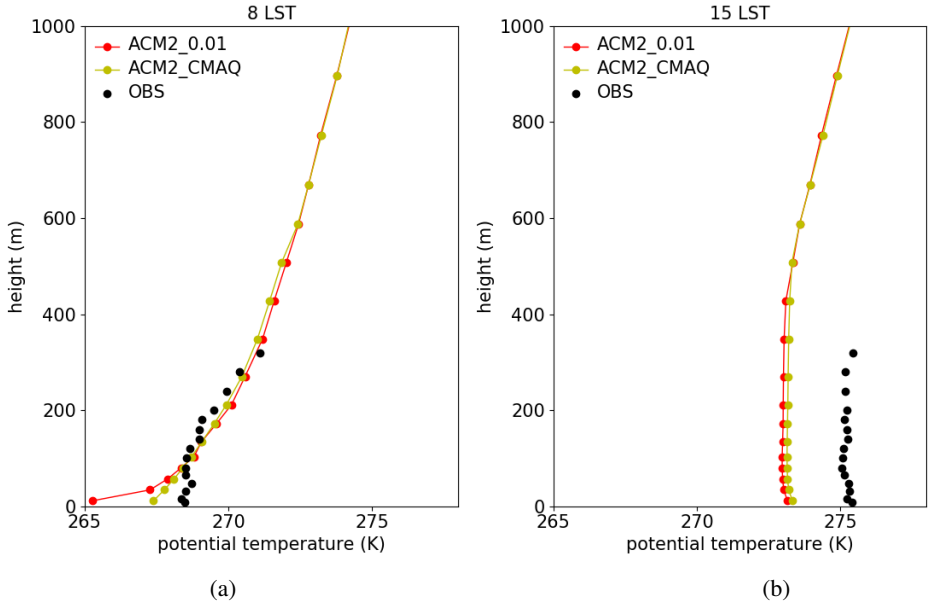

Figure 7. Hourly averaged vertical profiles of the potential temperature predicted by ACM2_0.01 and ACM2_CMAQ as well as the observations at (a) 8 LST and (b) 15 LST.

the same to that in the 8 LST simulation that above 500 m, the values of Kzmin given in ACM2_0.01 and ACM2_CMAQ are equal.

The spatial distribution of the time averaged differences of T2, TSK and HFX between ACM2_CMAQ and ACM2_0.01 is shown in Fig. 8. From Fig. 8(a)-(d), we can see that in urban areas, the difference in T2 and TSK between these two scenarios is mostly positive during both the daytime and the nighttime, which denotes that T2 and TSK predicted by ACM2_CMAQ are consistently higher than those predicted by ACM2_0.01 in urban areas. But in non-urban areas, the difference is minor. It is because that compared with ACM2_0.01, ACM2_CMAQ uses a larger Kzmin in urban and built-up areas below the height of 500 m. As a result, ACM2_CMAQ estimates a stronger vertical mixing in the PBL of urban areas than ACM2_0.01, thus resulting in an elevation of T2 and TSK. In contrast to that, in non-urban areas, the Kzmin values given in these two scenarios are identical (i.e. 0.01), the simulation reasults are thus similar. By comparing Fig. 8(a) and (b), it can also be found that in urban areas, the difference of T2 between ACM2_0.01 and ACM2_CMAQ during the nighttime is larger than that during the daytime, and this feature is also valid for the TSK deviation, according to Fig. 8(c) and (d). These results are consistent with the conclusions achieved above, stating that the change of Kzmin has the largest impact on the variation of T2 and TSK in the nighttime of the urban areas. With respect to HFX, it was found in Fig. 8(e) that during the daytime, the difference in HFX between ACM2_CMAQ and ACM2_0.01 is indiscernible. But in the nighttime (see Fig. 8f), the shapes of the urban areas are clearly indicated in the spatial distribution of the HFX deviation. It means that the HFX difference in urban areas between ACM2_0.01 and ACM2_CMAQ mostly exists during the nighttime. In addition, Fig. 8(f) also shows that during the nighttime,

https://doi.org/10.5194/gmd-2021-141
Preprint. Discussion started: 11 May 2021

Geoscientific Model Development
Discussions
Open Access
EGU

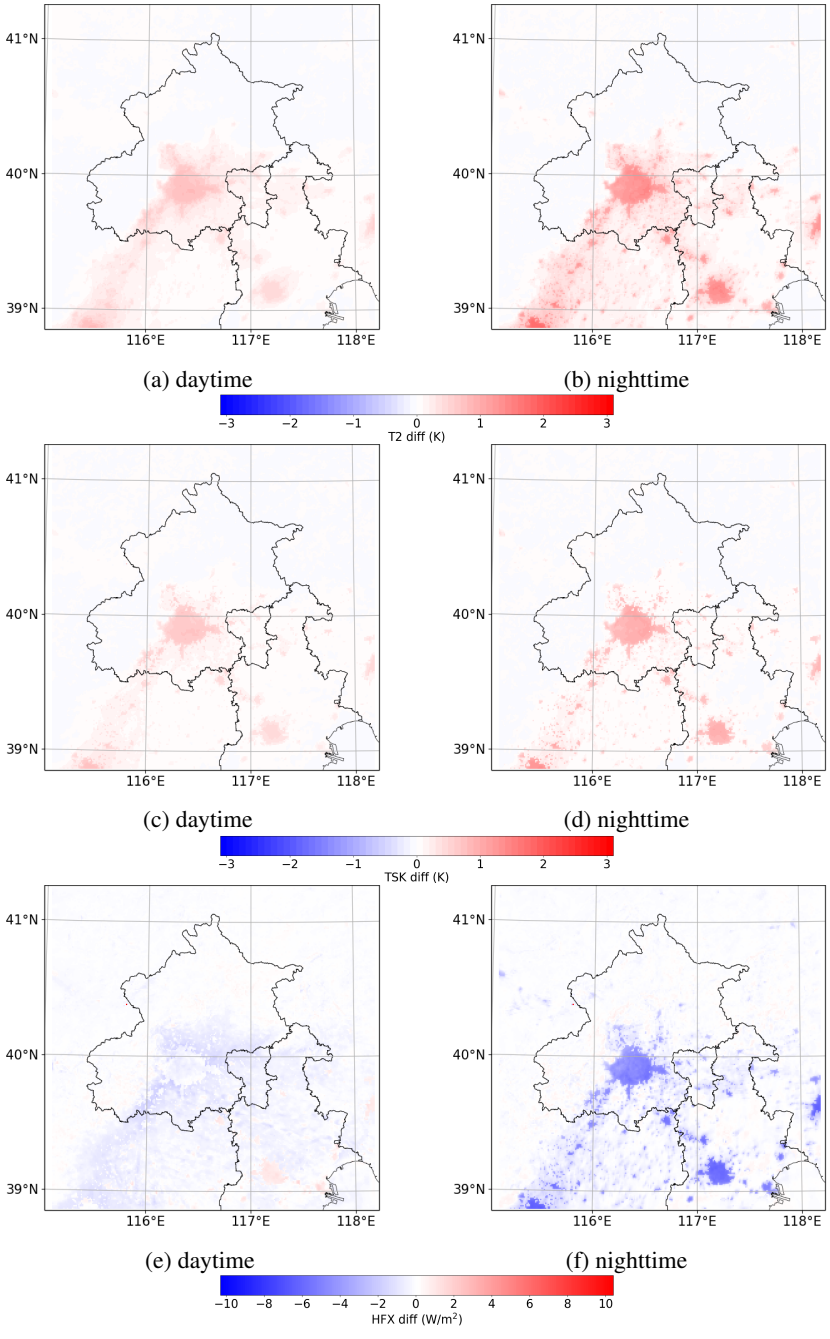

Figure 8. Spatial distribution of the mean differences (ACM2_CMAQ minus ACM2_0.01) in (a, b) T2, (c, d) TSK, and (e, f) HFX over the daytime (left row) and the nighttime (right row).

https://doi.org/10.5194/gmd-2021-141
Preprint. Discussion started: 11 May 2021


Geoscientific Model Development Discussions

the negative value of HFX in urban areas predicted by ACM2_CMAQ is lower than that provided by ACM2_0.01, which means that larger amount of heat is transferred from the atmosphere to the ground during the nighttime in the ACM2_CMAQ simulation.

4 Conclusions and Future Developments

In this study, we evaluated the performance of the ACM2 scheme with different Kzmin settings in the estimation of the 2-m temperature (T2), the surface skin temperature (TSK) and the near-surface air temperature (T_level1) in the area of Beijing, China. It was found that the change of Kzmin in the ACM2 scheme is able to significantly influence the performance of the model in simulating these temperatures. The increase of Kzmin leads to a remarkable elevation of T2 at night as well as a weakening of the diurnal change of T2. From the energy balance equation, we figured out that the mechanism for the elevation of T2 at night is because that larger Kzmin causes a significant enhancement of the turbulent mixing within the stable boundary layer at night. Then the enhanced mixing in the nighttime tends to reduce the vertical gradient of the potential temperature within the boundary layer, and thus elevate the air temperature near the ground surface (i.e. T_level1). The elevation of the near-surface air temperature then decreases the night sensible heat flux at the ground (i.e. HFX in the model), representing that larger heat is transferred from the atmosphere to the ground. As a result, the surface temperature (i.e. TSK) becomes higher. The interpolation of TSK and T_level1 in the model thus leads to the increase of the 2-m temperature (T2).

We also figured out the features about the influence of changing Kzmin on the temperature prediction under different underlying surface categories. It was found that the impact on the 2-m temperature and the surface temperature brought by the change of Kzmin is stronger during the nighttime than during the daytime, in plain areas than in mountain areas, in urban areas than in non-urban areas at night.

When using a function calculating Kzmin in the ACM2 scheme (i.e. the ACM2_CMAQ scenario), we found that the simulated 2-m temperature becomes higher in urban areas, compared with that using a constant Kzmin (i.e. ACM2_0.01). The reason is the same as that in the nighttime simulation, larger Kzmin in ACM2_CMAQ leads to a transport of more sensible heat from the atmosphere to the surface, resulting in a higher prediction of the 2-m temperature. The statistical parameters also show that ACM2_CMAQ preforms better than ACM2_0.01 in simulating the 2-m temperature of this region.

In addition, the simulated vertical profiles of the potential temperature show that ACM2_CMAQ estimates a smaller potential temperature gradient than ACM2_0.01 within the boundary layer, especially at night, and the profile of the potential temperature given by ACM2_CMAQ is closer to the observation compared with that given by ACM2_0.01. Moreover, the spatial distribution of the temperature deviation between these two scenarios shows that in the daytime, the temperature simulated by ACM2_CMAQ is only slightly higher than ACM2_0.01 in both urban and non-urban areas. But the difference becomes remarkable in the nighttime of the urban areas.

In the future, longer time periods are to be simulated so that the conclusions achieved in the present study can be verified more thoroughly. Moreover, the impacts of changing Kzmin on the spatiotemporal distribution of other meteorological parameters such the wind and the moisture will also be evaluated. In addition, we plan to assess the effects of changing Kzmin

https://doi.org/10.5194/gmd-2021-141
Preprint. Discussion started: 11 May 2021

on simulations of the air pollution under different weather conditions, due to the strong connection between the diffusion of pollutants and the vertical turbulent mixing.

Code and data availability. The source code of WRF version 3.9.1.1 can be found on the website: www2.mmm.ucar.edu/wrf/users/download/. The code described by Eqs. (3)–(7), defining a functional type Kzmin in the ACM2 scheme of WRF, can be found in the directory named "Modified_WRF_Code" in the supplementary material of the present manuscript. The WRF model input namelist file and the post-processing python scripts are also available in the supplements, named "WRF_namelist" and "post-processing-scripts", respectively. In addition, the observational data obtained from the meteorological observation tower as well as the observational system, provided by the Institute of Atmospheric Physics, Chinese Academy Sciences (IAP, CAS), are included in the directory "obs_data" of the supplements.

Acknowledgements. This work was financially supported by the National Key R&D Program of China (Grant No. 2017YFC0209801) and the National Natural Science Foundation of China (Grant No. 41375044). The numerical calculations in this paper have been done on the high performance computing system in the High Performance Computing Center, Nanjing University of Information Science & Technology.

Author contributions. Hongyi Ding and Le Cao conceived the idea of the article and ran the model. Hongyi Ding also wrote the python script for the data processing. Le Cao and Hongyi Ding wrote the paper together. Haimei Jiang and Wenxing Jia revised the paper and gave valuable suggestions. Yong Chen and Junling An from IAP, CAS provided the observational data and gave useful advice on the comparison of the model results with the observations. All the authors listed have read and approved the final manuscript.

Competing interests. The authors declare no conflict of interest.

https://doi.org/10.5194/gmd-2021-141
Preprint. Discussion started: 11 May 2021

Geoscientific Model Development Discussions

References

Banks, R. F., Tiana-Alsina, J., Baldasano, J. M., Rocadenbosch, F., Papayannis, A., Solomos, S., and Tzanis, C. G.: Sensitivity of boundary-layer variables to PBL schemes in the WRF model based on surface meteorological observations, lidar, and radiosondes during the HygrA-CD campaign, Atmospheric Research, 176, 185–201, 2016.

Bougeault, P. and Lacarrere, P.: Parameterization of orography-induced turbulence in a mesobeta–scale model, Monthly Weather Review, 117, 1872–1890, 1989.

Broxton, P. D., Zeng, X., Sulla-Menashe, D., and Troch, P. A.: A global land cover climatology using MODIS data, Journal of Applied Meteorology and Climatology, 53, 1593–1605, 2014.

Byun, D. and Schere, K. L.: Review of the Governing Equations, Computational Algorithms, and Other Components of the Models-3 Community Multiscale Air Quality (CMAQ) Modeling System, Applied Mechanics Reviews, 59, 51–77, 2006.

Chaouch, N., Temimi, M., Weston, M., and Ghedira, H.: Sensitivity of the meteorological model WRF-ARW to planetary boundary layer schemes during fog conditions in a coastal arid region, Atmospheric Research, 187, 106–127, 2017.

Chen, F. and Dudhia, J.: Coupling an advanced land surface–hydrology model with the Penn State–NCAR MM5 modeling system. Part I: Model implementation and sensitivity, Monthly Weather Review, 129, 569–585, 2001.

Chen, S.-H. and Sun, W.-Y.: A one-dimensional time dependent cloud model, Journal of the Meteorological Society of Japan. Ser. II, 80, 99–118, 2002.

Cuchiara, G. C., Li, X., Carvalho, J., and Rappenglück, B.: Intercomparison of planetary boundary layer parameterization and its impacts on surface ozone concentration in the WRF/Chem model for a case study in Houston/Texas, Atmospheric Environment, 96, 175–185, 2014.

Du, Q., Zhao, C., Zhang, M., Dong, X., Chen, Y., Liu, Z., Hu, Z., Zhang, Q., Li, Y., Yuan, R., and Miao, S.: Modeling diurnal variation of surface $PM_{2.5}$ concentrations over East China with WRF-Chem: impacts from boundary-layer mixing and anthropogenic emission, Atmospheric Chemistry and Physics, 20, 2839–2863, 2020.

Dudhia, J.: Numerical study of convection observed during the winter monsoon experiment using a mesoscale two-dimensional model, Journal of the Atmospheric Sciences, 46, 3077–3107, 1989.

Grell, G. A. and Dévényi, D.: A generalized approach to parameterizing convection combining ensemble and data assimilation techniques, Geophysical Research Letters, 29, 38–1, 2002.

Grell, G. A., Peckham, S. E., Schmitz, R., McKeen, S. A., Frost, G., Skamarock, W. C., and Eder, B.: Fully coupled “online” chemistry within the WRF model, Atmos. Environ., 39, 6957 – 6975, 2005.

Gunwani, P. and Mohan, M.: Sensitivity of WRF model estimates to various PBL parameterizations in different climatic zones over India, Atmospheric Research, 194, 43–65, 2017.

Hong, S.-Y. and Pan, H.-L.: Nonlocal boundary layer vertical diffusion in a medium-range forecast model, Monthly Weather Review, 124, 2322–2339, 1996.

Hong, S.-Y., Noh, Y., and Dudhia, J.: A new vertical diffusion package with an explicit treatment of entrainment processes, Monthly Weather Review, 134, 2318–2341, 2006.

Hu, X.-M., Nielsen-Gammon, J. W., and Zhang, F.: Evaluation of three planetary boundary layer schemes in the WRF model, Journal of Applied Meteorology and Climatology, 49, 1831–1844, 2010.

Janjić, Z. I.: The step-mountain eta coordinate model: Further developments of the convection, viscous sublayer, and turbulence closure schemes, Monthly Weather Review, 122, 927–945, 1994.

https://doi.org/10.5194/gmd-2021-141
Preprint. Discussion started: 11 May 2021

Li, X. and Rappenglueck, B.: A study of model nighttime ozone bias in air quality modeling, Atmospheric Environment, 195, 210–228, 2018.

Madala, S., Satyanarayana, A., and Rao, T. N.: Performance evaluation of PBL and cumulus parameterization schemes of WRF ARW model in simulating severe thunderstorm events over Gadanki MST radar facility—case study, Atmospheric Research, 139, 1–17, 2014.

Mlawer, E. J., Taubman, S. J., Brown, P. D., Iacono, M. J., and Clough, S. A.: Radiative transfer for inhomogeneous atmospheres: RRTM, a validated correlated-k model for the longwave, Journal of Geophysical Research: Atmospheres, 102, 16 663–16 682, 1997.

Moeng, C.-H., Dudhia, J., Klemp, J., and Sullivan, P.: Examining Two-Way Grid Nesting for Large Eddy Simulation of the PBL Using the WRF Model, Monthly Weather Review, 135, 2295 – 2311, 2007.

Monin, A. S. and Obukhov, A. M.: Basic laws of turbulent mixing in the ground layer of the atmosphere, Tr. Akad. Nauk SSSR Geofiz. Inst, 24, 163–187, 1954.

National Centers for Environmental Prediction, National Weather Service, NOAA, U.S. Department of Commerce: NCEP FNL Operational Model Global Tropospheric Analyses, continuing from July 1999, 2000.

Nielsen-Gammon, J. W., Hu, X.-M., Zhang, F., and Pleim, J. E.: Evaluation of planetary boundary layer scheme sensitivities for the purpose of parameter estimation, Monthly Weather Review, 138, 3400–3417, 2010.

Pleim, J. E.: A combined local and nonlocal closure model for the atmospheric boundary layer. Part I: Model description and testing, Journal of Applied Meteorology and Climatology, 46, 1383–1395, 2007a.

Pleim, J. E.: A combined local and nonlocal closure model for the atmospheric boundary layer. Part II: Application and evaluation in a mesoscale meteorological model, Journal of Applied Meteorology and Climatology, 46, 1396–1409, 2007b.

Pleim, J. E. and Chang, J. S.: A non-local closure model for vertical mixing in the convective boundary layer, Atmospheric Environment. Part A. General Topics, 26, 965–981, 1992.

Poulos, G., Blumen, W., Fritts, D., Lundquist, J., Sun, J., Burns, S., Nappo, C., Banta, R., Newsom, R., Cuxart, J., Terradellas, E., and Balsley, B.: CASES99: A Comprehensive Investigation of the Stable Nocturnal Boundary Layer, Bulletin of The American Meteorological Society - BULL AMER METEOROL SOC, 83, 2002.

Shin, H. H. and Hong, S.-Y.: Intercomparison of planetary boundary-layer parametrizations in the WRF model for a single day from CASES-99, Boundary-Layer Meteorology, 139, 261–281, 2011.

Skamarock, W., Klemp, J., Dudhia, J., Gill, D., Barker, D., Wang, W., and Powers, J.: A Description of the Advanced Research WRF Version 3, NCAR Technical Note, Tech. Rep. NCAR/TN–475+STR, National Center for Atmospheric Research, Boulder, CO, 2008.

Steeneveld, G., Van de Wiel, B., and Holtslag, A.: Modelling the Arctic stable boundary layer and its coupling to the surface, Boundary-layer meteorology, 118, 357–378, 2006.

Stull, R. B.: An Introduction to Boundary Layer Meteorology, vol. 13, Springer Science & Business Media, 1988.

Sukoriansky, S. and Galperin, B.: A Quasi-Normal Scale Elimination Theory of Turbulent Flows With Stable Stratification, in: Volume 4: Fatigue and Fracture; Fluids Engineering; Heat Transfer; Mechatronics; Micro and Nano Technology; Optical Engineering; Robotics; Systems Engineering; Industrial Applications, Engineering Systems Design and Analysis, pp. 179–183, 2008.

Sukoriansky, S., Galperin, B., and Perov, V.: A quasi-normal scale elimination model of turbulence and its application to stably stratified flows, Nonlinear Processes in Geophysics, 13, 9–22, 2006.

Udina, M., Sun, J., Kosović, B., and Soler, M. R.: Exploring vertical turbulence structure in neutrally and stably stratified flows using the weather research and forecasting–large-eddy simulation (WRF–LES) model, Boundary-Layer Meteorology, 161, 355–374, 2016.

https://doi.org/10.5194/gmd-2021-141
Preprint. Discussion started: 11 May 2021

Willmott, C. J.: Some comments on the evaluation of model performance, Bulletin of the American Meteorological Society, 63, 1309–1313, 1982.

Xie, B., Fung, J. C., Chan, A., and Lau, A.: Evaluation of nonlocal and local planetary boundary layer schemes in the WRF model, Journal of Geophysical Research: Atmospheres, 117, 2012.

Zhang, D. and Anthes, R. A.: A high-resolution model of the planetary boundary layer—Sensitivity tests and comparisons with SESAME-79 data, Journal of Applied Meteorology, 21, 1594–1609, 1982.